 SID, vol.1, no.1, pp.67-82, 2005

Numerical Analysis of Damage Evolution in Ductile Solids

M. Mashayekhi[1], S. Ziaei-Rad[2], J. Parvizian[3], K. Nikbin[1] and H. Hadavinia[1]

Abstract: The continuum mechanical simulation of microstructural damage process is important in the study of ductile fracture mechanics. An essential feature in these analyses, is the strong influence of stress triaxiality ratio, i.e. the ratio of mean stress to equivalent stress, on the rate of damage growth. In this paper, finite element simulation of damage evolution and fracture initiation in ductile solids will be investigated. A fully coupled constitutive elastic-plastic-damage model has been implemented. The stress update algorithm for the constitutive model is presented together with the consistent tangent operator, which is needed for implicit FEA. Simulations are performed and the results are compared with the numerical and experimental ones in the literature and good agreements were found between them.

keyword: Ductile fracture, Continuum damage, Triaxiality

Nomenclature

A total cross sectional area

A_D damaged area

D damage variable

$\dot{D}$ damage rate

E Young's modulus

$\mathbf{e}$ strain deviator tensor

G shear moduli

K bulk moduli

p hydrostatic pressure

R radial growth of the yield surface

r damage parameters

s damage parameter and entropy

$\mathbf{s}$ deviatoric stress tensor

$\tilde{\mathbf{s}}$ deviatoric stress tensor based on effective stress

T temperature

v volumetric strain

Y damage energy release rate

$\boldsymbol{\varepsilon}$ strain tensor

$\dot{\boldsymbol{\varepsilon}}^p$ plastic strain tensor rate

$\dot{\varepsilon}^p_{eq}$ equivalent plastic strain rate

Φ yield function

$\dot{\gamma}$ plastic consistency parameter

ν Poisson's ratio

$\boldsymbol{\sigma}$ Cauchy stress tensor

$\tilde{\boldsymbol{\sigma}}$ effective stress tensor

σ_{eq} equivalent stress

σ^0_Y initial yield stress

Ψ potential of dissipation

[1] Mechanical Engineering Department
Imperial College London
South Kensington Campus
SW7 2AZ, UK

[2] Mechanical Engineering Department
Isfahan University of Technology
Isfahan, Iran

[3] Industrial Engineering Department
Isfahan University of Technology
Isfahan, Iran

1 Introduction

Damage of materials means the progressive or sudden deterioration of their mechanical strength due to loading, thermal or chemical effects. It could cover all related phenomena that occur from the virgin or reference state up to a mesocrack initiation. Form a physical point of view, damage can originate from multiple causes: debonding of atoms, nucleation, or growth and coalescence of microcracks and microcavitities. Despite the discontinuous nature of such processes at the microscale, it is possible to model the process at the microscale as continuous. Thus homogeneous modelling in which microcracks and/or microvoids are represented by a continuous variable in the sense of the mechanics of continuous media can be performed [Lemaitre (2001)].

Over the last two decades, the study of large deforma-

tions in metals has revealed the phenomenon of initiation and growth of microvoids, cavities and microcracks in the process of "ductile plastic damage". Considerable efforts have been concentrated on the modelling of the gradual internal deterioration (or damage), which is frequently accompanied by the occurrence of macroscopic failure in common engineering materials [de Souza Neto, et al. (1994)]. Within the framework of continuum thermodynamics, this phenomenon have been described by several phenomenological or micromechanical based continuum damage models (CDM). Initially, the development and application of damage models was focused on ductile fracture. However, in recent years, several different formulations for a variety of materials and processes have been presented, such as brittle [Krajcinovic, et al. (1981); Krajcinovic (1983); Simo and Ju (1987a, b)], elastic–brittle [Murakami (1988); Murakami, Kamiya (1997)], creep[Chaboche (1988a, b); Lemaitre (1984); Krajcinovic, et al. (1984); Saanouni, et al. (1986); Murakami (1990)], fatigue and creep-fatigue [Chaboche (1988b); Lemaitre (1984)] among others. Hence, the application range of the continuum damage theory has been widened.

As experimentally verified for many materials [Lemaitre (1984)], especially close to material failure, the energy dissipation associated with the nucleation and growth of voids and microcracks, which accompany large plastic flow, has a dominant effect. This fact suggests that the prediction of rupture as well as final material properties demands consideration of coupling between plastic flow and damage at the constitutive level.

In this paper, a model based on the work of de Souza Neto [de Souza Neto (2002)] and later by Andrade Pires *et al* [Andrade Pires, et al. (2003)] is formulated. Based on the fact that whenever load reversal is absent or negligible, kinematic hardening plays no practical role and the original Lemaitre model can be safely simplified with a version that ignores the kinematic contribution to overall hardening, in the model the kinematics hardening in the original Lemaitre damage model is disregarded and a constitutive integration algorithm is deduced in which the return mapping procedure under any stress state is reduced to the solution of a single non-linear equation. Using the model, two examples are presented in this paper and the results are verified by experiments.

2 Elements of continuous damage mechanics

At the microscale level, damage may be interpreted as the creation of microsurfaces of discontinuities: breaking of atomic bonds and plastic enlargement of microcavities. At the mesoscale, the number of broken bonds or the pattern of microcavities may be approximated in any plane by the area of the intersections of the flaws with that plane. The original model by Kachanov [Kachanov (1958)] postulated that the loss of stiffness and integrity attributed to microcracks can be measured by a macroscopic damage parameter, D. This dimensionless damage parameter defined by scaling the net area by the total cross sectional area of the representative volume element (RVE). More specifically, the history of inelastic deformation and its change may be defined by the evolution of this internal variable that depends on the expected value of micro-defect density. This important parameter is continuous in the sense of continuum mechanics and it is representative of the failure of microdefects over the mesoscale volume element. Such microscopic defects are assumed isotropically distributed, and in the present model, they will be phenomenologically reflected by the degradation of the elastic modulus. In essence, it is similar to the plastic strain, ε_p, in plasticity which represents the average of many slips bands.

In a simple one dimensional case of a homogeneous damage, the definition of damage parameter as the effective surface density of micro-defects can be written as

$$D = \frac{A_D}{A} \tag{1}$$

where A_D is the damaged area and A is the total cross sectional area. It follows from this definition that the value of the scalar variable D is bounded by $0 \leq D \leq 1$ where $D = 0$ is representative of undamaged state; and $D = 1$ is representative of rupture. In fact, the failure occurs for $D < 1$ through a process of instability.

In order to model elasticity, thermal effects and plasticity with damage within the hypothesis of isotropy, the variables referred in Table 1 have to be introduced [Lemaitre (1985a, b)] where R is the scalar variable associated with isotropic hardening.

3 Standard Lemaitre damage model

As explained in Section 2, in the Lemaitre damage model [Lemaitre (1985a, b; 1996)], the damage variable is de-

Table 1 : Thermodynamic variables

Observable variables	Internal variables	Associated variables
Elastic strain tensor $\boldsymbol{\varepsilon}^e$		Stress tensor $\boldsymbol{\sigma}$
Temperature T		Entropy s
	Accumulated plastic strain ε^p_{eq}	Radius of the yield surface R
	Damage D	Damage strain energy release rate Y

fined as the net area of a unit surface cut by a given plane corrected for the presence of existing cracks and cavities. By assuming homogeneous distribution of microvoids and the hypothesis of strain equivalence, which states that the strain behaviour of a damaged material is represented by constitutive equations of the virgin material (without damage) in the potential of which the stress is simply replaced by the effective stress [Lemaitre (1985a, b; 1996)], the effective stress tensor, $\tilde{\boldsymbol{\sigma}}$, can be represented as

$$\tilde{\boldsymbol{\sigma}} = \frac{\boldsymbol{\sigma}}{1-D} \tag{2}$$

where $\boldsymbol{\sigma}$ is the stress tensor for the undamaged material. The corresponding effective stress deviator, $\tilde{\mathbf{s}}$, is related to the stress deviator, $\mathbf{s}$, by an analogous expression:

$$\tilde{\mathbf{s}} = \frac{\mathbf{s}}{1-D} \tag{3}$$

The thermodynamic theory of irreversible process with internal variables provides a consistent framework for the development of evolution and constitutive equations for elastic-plastic-damage materials. The thermodynamic of irreversible process defines thermodynamical force (R,Y) such that the specific intrinsic dissipated power is

$$\boldsymbol{\sigma} : \dot{\boldsymbol{\varepsilon}}^p - R\,\dot{\varepsilon}^p_{eq} - Y\dot{D} \;\geq\; 0 \tag{4}$$

where $\dot{\boldsymbol{\varepsilon}}^p$ is the plastic strain tensor and $\dot{\varepsilon}^p_{eq}$ is the equivalent plastic strain rate, $\dot{\varepsilon}^p_{eq} = \sqrt{2/3}\,\|\dot{\boldsymbol{\varepsilon}}^p\|$. The damage energy release rate, $-Y$, corresponds to the variation of internal energy density due to damage growth at constant stress which is the continuum damage analogue of the J-integral used in fracture mechanics [Lemaitre (1985a)]. The term $-Y\dot{D}$ is the power dissipated by the process of internal deterioration (mainly as decohesion of interatomic bonds). Therefore, the evolution equation for internal variables can be derived by assuming the existence of a potential of dissipation, Ψ, as a scalar convex function of the state variables, which is decomposed into plastic, Ψ^p, and damage, Ψ^d, components as

$$\Psi = \Psi^p + \Psi^d = \Phi + \frac{r}{(1-D)(s+1)}\left(\frac{-Y}{r}\right)^{s+1} \tag{5}$$

for a process accounting for isotropic hardening and isotropic damage, in which r and s are material and temperature-dependent properties and Φ and Y are, respectively, the yield function and the damage strain energy release rate, given by

$$\Phi(\boldsymbol{\sigma},\ \varepsilon^p_{eq}, D) = \frac{\sigma_{eq}}{(1-D)} - [\sigma^0_Y + R(\varepsilon^p_{eq})] \tag{6}$$

and

$$-Y = \frac{\sigma^2_{eq}}{2E(1-D)^2}\left[\frac{2}{3}(1+\nu) + 3(1-2\nu)\left(\frac{p}{\sigma_{eq}}\right)^2\right] \tag{7}$$

where σ^0_Y is the initial yield stress, R represents the radial growth (or shrinking) of the yield surface, σ_{eq} is the equivalent stress, $\sigma_{eq} = \sqrt{3/2}\,\|\mathbf{s}\|$, $p = (1/3)tr(\boldsymbol{\sigma})$, E is the Young's modulus and ν is Poisson's ratio.

By the hypothesis of generalized normality, the plastic flow equation is

$$\dot{\boldsymbol{\varepsilon}}^p = \dot{\gamma}\sqrt{\frac{3}{2}}\frac{\mathbf{s}}{\|\mathbf{s}\|} = \dot{\gamma}\frac{3}{2}\frac{\mathbf{s}}{\sigma_{eq}} \tag{8}$$

and the evolution law of the internal variables are

$$\begin{aligned} \dot{\varepsilon}^p_{eq} &= -\dot{\gamma}\frac{\partial\Psi}{\partial R} = \dot{\gamma} \\ \dot{D} &= -\dot{\gamma}\frac{\partial\Psi}{\partial Y} = \dot{\gamma}\frac{1}{1-D}\left(\frac{-Y}{r}\right)^s \end{aligned} \tag{9}$$

where $\dot{\gamma}$ is the plastic consistency parameter, which is subject to the so-called Kuhn-Tucker conditions for loading and unloading as

$$\dot{\gamma} \geq 0, \qquad \Phi \leq 0, \quad \dot{\gamma}\Phi = 0 \tag{10}$$

The evolution problem is highly non-linear thereby requiring an efficient integration algorithm, as discussed in Section 4.

4 Numerical integration for damage materials

An algorithm for the numerical integration of the above elastic-plastic-damage constitutive equations will be presented in this section. Algorithms based on the operator split concept, resulting in the standard elastic predictor/plastic corrector format, are widely used in computational plasticity [Simo and Hughes (1998)]. Let us consider what happens to a typical Gauss point of the finite element mesh within a (pseudo-) time interval $[t_n,\ t_{n+1}]$.

Given the incremental strain:

$$\Delta\boldsymbol{\varepsilon} = \boldsymbol{\varepsilon}_{n+1} - \boldsymbol{\varepsilon}_n \tag{11}$$

and the values $\boldsymbol{\sigma}_n$, $\boldsymbol{\varepsilon}^p_n$, $\varepsilon^p_{eq,n}$ and D_n at t_n, the numerical integration algorithm should obtain the updated values at the end of the interval, $\boldsymbol{\sigma}_{n+1}$, $\boldsymbol{\varepsilon}^p_{n+1}$, $\varepsilon^p_{eq,n+1}$ and D_{n+1} such that they become consistent with the constitutive equations of the model.

The first step in the algorithm is the evaluation of the elastic trial state in which the increment is assumed to be purely elastic with no evolution of internal variables (internal variables frozen at t_n). The elastic trial strain and trial accumulated plastic strain are given by

$$\boldsymbol{\varepsilon}^{e,trial}_{n+1} = \boldsymbol{\varepsilon}^e_n + \Delta\boldsymbol{\varepsilon}\,, \qquad \varepsilon^{p,trial}_{eq,\,n+1} = \varepsilon^p_{eq,\,n} \tag{12}$$

The corresponding elastic trial stress tensor is computed from

$$\boldsymbol{\sigma}^{trial} = \boldsymbol{\sigma}_n + \mathbf{E} : \Delta\boldsymbol{\varepsilon} \tag{13}$$

Where $\mathbf{E}$ is the standard isotropic elasticity tensor. Equation (13) can be splitted to deviator/hydrostatic part of $\boldsymbol{\sigma}$ as

$$\mathbf{s}^{trial} = \mathbf{s}_n + 2G\Delta\mathbf{e} \qquad p^{trial} = p_n + K\Delta v \tag{14}$$

where G and K are, respectively, the shear and bulk moduli, $\mathbf{e}$ and v denote, respectively, the strain deviator and the volumetric strain and p stands for the hydrostatic stress.

The next step of the algorithm is to check for plastic consistency. With variables $\varepsilon^p_{eq,\,n}$ and D frozen at time t_n we compute

$$\Phi^{trial} = \sqrt{\frac{3}{2}}\frac{\left\|\mathbf{s}^{\mathbf{trial}}\right\|}{(1-D_n)} - [\sigma^0_Y + R(\varepsilon^p_{eq,n})] \tag{15}$$

If $\Phi^{trial} \le 0$, then there is no plastic flow or damage evolution within the interval and

$$\boldsymbol{\sigma}_{n+1} = \boldsymbol{\sigma}^{trial}, \quad \varepsilon^p_{eq,\,n+1} = \varepsilon^p_{eq,n}, \qquad D_{n+1} = D_n \tag{16}$$

Otherwise, the plastic corrector (or return mapping algorithm) should be applied, i.e., the evolution equations for $\boldsymbol{\varepsilon}^p$, $\varepsilon^p_{eq,n}$ and D must be integrated numerically having the trial state as the initial condition. Using a standard backward Euler approximation, the discrete counterparts of equations (8) and (9) becomes

$$\boldsymbol{\varepsilon}^p_{n+1} = \boldsymbol{\varepsilon}^p_n + \Delta\gamma\sqrt{\frac{3}{2}}\frac{\mathbf{s}^{trial}}{\|\mathbf{s}^{trial}\|} \tag{17}$$

and

$$\begin{aligned}\varepsilon^p_{eq,\,n+1} &= \varepsilon^p_{eq,n} + \Delta\gamma \\ D_{n+1} &= D_n + \frac{\Delta\gamma}{1-D_{n+1}}\left(\frac{-Y_{n+1}}{r}\right)^s\end{aligned} \tag{18}$$

The above equations must be complemented by the consistency condition that guarantees the stress state at the end of a plastic step lies on the updated yield surface; i.e.

$$\Phi_{n+1} = \sqrt{\frac{3}{2}}\frac{\|\mathbf{s}_{n+1}\|}{(1-D_{n+1})} - [\sigma^0_Y + R(\varepsilon^p_{eq,n+1})] = 0 \tag{19}$$

From standard arguments used in the derivation of return mapping algorithms [Simo and Hughes (1998)], the system of discretised equations (17) and (18) can be reduced to the following scalar non-linear equation for the incremental plastic multiplier $\Delta\gamma$

$$\begin{aligned}&\sqrt{\frac{3}{2}}\left\|\mathbf{s}^{trial}\right\| - 3G\Delta\gamma \\ &-(1-D_{n+1})[\sigma^0_Y + R(\varepsilon^p_{eq,n} + \Delta\gamma)] = 0\end{aligned} \tag{20}$$

or, equivalently,

$$D_{n+1} = D(\Delta\gamma) \equiv 1 - \frac{\sqrt{\frac{3}{2}}\left\|\mathbf{s}^{trial}\right\| - 3G\Delta\gamma}{[\sigma^0_Y + R(\varepsilon^p_{eq,n} + \Delta\gamma)]} \tag{21}$$

which expresses D_{n+1} as an explicit function of $\Delta\gamma$.

In summary, the return mapping has been reduced to the set of two scalar equations comprising (18) and (21). The unknowns of this system of equations are $\Delta\gamma$ and D_{n+1}. After solution, $\Delta\gamma$ and D_{n+1} are updated. This two-equation return mapping has been proposed by Vaz Jr (2001) in the context of fracture prediction in metal cutting processes. de Souza Neto (2002) has shown how the above system can be further reduced leading to a computationally more efficient single-equation return mapping algorithm for the unknown $\Delta\gamma$

$$D(\Delta\gamma) - D_n - \frac{\Delta\gamma}{1-D(\Delta\gamma)}\left(\frac{-Y(\Delta\gamma)}{r}\right)^s = 0 \tag{22}$$

In (22), the dependency of Y on $\Delta\gamma$ originates from its dependency on the updated values of D and $\boldsymbol{\sigma}$ (clearly shown in definition (7)). The updated stress tensor, $\boldsymbol{\sigma}_{n+1}$, is obtained as

$$\boldsymbol{\sigma}_{n+1} = \mathbf{s}_{n+1} + p_{n+1}\mathbf{I} \tag{23}$$

where $\mathbf{I}$ is the second order identity tensor and $\mathbf{s_{n+1}}$ is obtained from the standard implicit Mises return mapping as a function of $\Delta\gamma$ according to update formula:

$$\mathbf{s}_{n+1} = \left(1 - \sqrt{\frac{3}{2}}\frac{2G\Delta\gamma}{\|\mathbf{s}^{trial}\|}\right)\mathbf{s}^{trial}, \qquad p_{n+1} = p^{trial} \tag{24}$$

The solution of (22) is undertaken by the standard Newton–Raphson iterative scheme.

5 Summary of the algorithm

Elastic predictor/return mapping algorithm for the elastic-plastic-damage model can be summarised as following:

Step1. Elastic predictor: Given the incremental strain, $\Delta\boldsymbol{\varepsilon}$, and the state variables at t_n, compute elastic trial stresses:

$$\begin{aligned}
&\boldsymbol{\varepsilon}^{e\,trial}_{n+1} = \boldsymbol{\varepsilon}^{e}_{n} + \Delta\boldsymbol{\varepsilon}\\
&\varepsilon^{p\,trial}_{eq,\,n+1} = \varepsilon^{p}_{eq,n}\\
&\mathbf{s}^{trial} = \mathbf{s}_n + 2G\Delta\mathbf{e}\\
&p^{trial} = p_n + K\Delta v \quad D_{n+1} = D_n.
\end{aligned}$$

Step 2. Plastic consistency check: First compute

$$\Phi^{trial} = \sqrt{\frac{3}{2}}\frac{\|\mathbf{s}^{trial}\|}{(1-D_n)} - [\sigma^0_Y + R(\varepsilon^p_{eq,n})],$$

and then check:

IF $\Phi^{trial} \le \varepsilon_{tol}$ **THEN** (Elastic state)

Update $(\cdot)_{n+1} = (\cdot)^{trial}$ **RETURN**

ELSE (Plastic state)

Step 3. Return mapping: Find $\Delta\gamma$ such that

$$D(\Delta\gamma) - D_n - \frac{\Delta\gamma}{1-D(\Delta\gamma)}\left(\frac{-Y(\Delta\gamma)}{r}\right)^s = 0$$

where $D(\Delta\gamma)$ and $Y(\Delta\gamma)$ are defined, respectively by (21) and (7).

Step 4. Update the variable:

$$\mathbf{s}_{n+1} = \left(1 - \sqrt{\frac{3}{2}}\frac{2G\Delta\gamma}{\|\mathbf{s}^{trial}\|}\right)\mathbf{s}^{trial}, \qquad p_{n+1} = p^{trial},$$

$$\boldsymbol{\sigma}_{n+1} = \mathbf{s}_{n+1} + p_{n+1}\mathbf{I}, \quad \varepsilon^p_{eq,\,n+1} = \varepsilon^p_{eq,n} + \Delta\gamma$$

$$\boldsymbol{\varepsilon}^e_{n+1} = \frac{1}{2G}\mathbf{s}_{n+1} + \frac{1}{3K}p_{n+1}\mathbf{I}, \qquad D_{n+1} = D(\Delta\gamma)$$

ENDIF

RETURN

Summary of the above algorithm is presented in Figure 1.

6 Numerical examples

The present model has been verified by solving two numerical examples using the finite element code ABAQUS/standard (2003) in two- and three-dimensional solid elements. The first example is the simulation of a two- and three-dimensional tensile test on a specimen subjected to a monotonic axial stretching. In the second example, the simulation of a three point bending test was investigated.

6.1 Tensile Test

The classical tensile test of a rectangular bar specimen is used to apply the presented damage model. Tensile tests have been extensively used in both experimental and numerical analyses of ductile fracture. In this problem, a specimen under tensile loading experiences a characteristic stress–strain behaviour, which causes the fracture to initiate at its centre and propagate towards the outer edge [Hancock and Mackenzie (1976)]. On a microscopic scale, nucleation, growth and coalescence of microvoids were found to be the mechanism, which causes fracture.

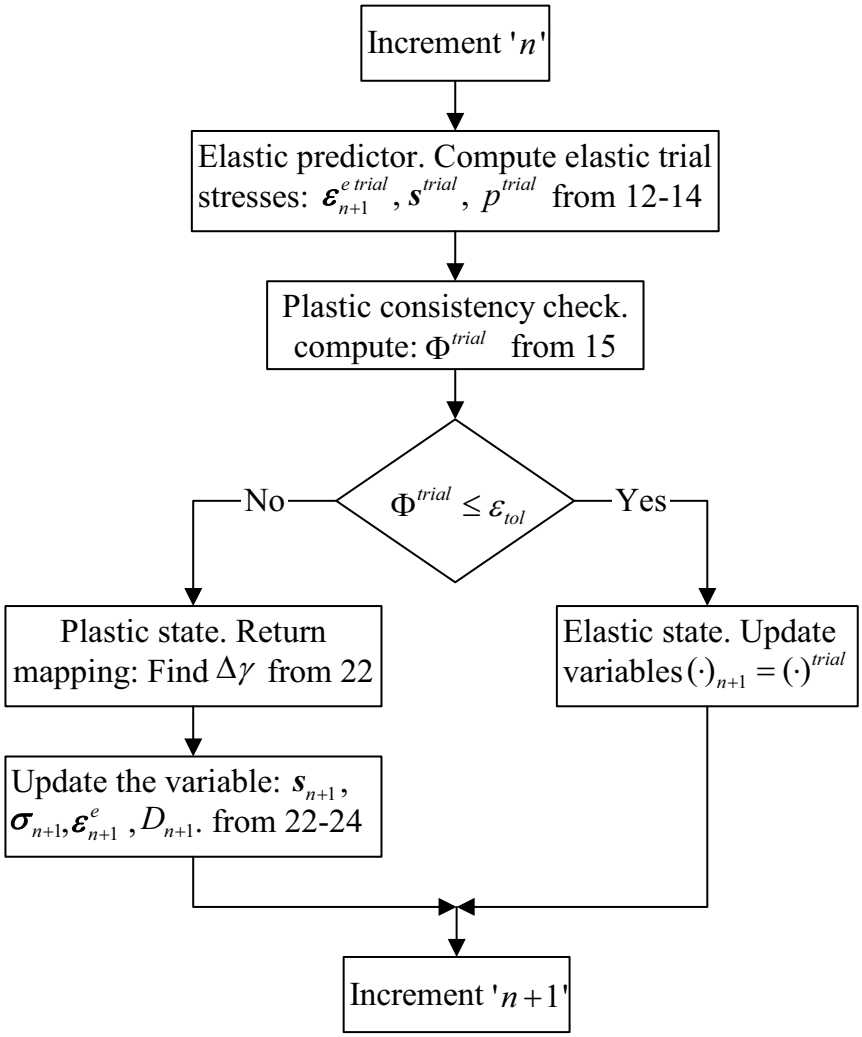

Figure 1 : Flow chart of elastic predictor/return mapping algorithm for the elastic-plastic-damage model.

Numerical analysis for the classical tensile test of an axisymmetric notched bar specimen have been carried out by de Souza Neto (2002) and Vaz Jr. and Owen (2001). In the present study two- and three-dimensional rectangular section tensile specimen were analysed. The geometry of the problem, boundary conditions and the finite element mesh for both two- and three-dimensional cases are shown in Figure 2 and are based on ASTM standard. The mesh discretises one symmetric quarter of the sample with appropriate symmetric boundary conditions imposed to the relevant edges. The loading consists of a prescribed monotonically increasing axial displacement of the nodes on the end face of the mesh, as shown in Figure 2. The material properties were adopted from [Benallal, et al. (1987)] and presented in Table 2. In the present analysis, displacement control was incrementally applied to the end of the specimen. When the damage at any Gauss point in the structure for the first time reached 0.9, the simulation was terminated. This state was reached with a prescribed end displacement of 4.3 mm in two-dimensional case and 5.59 mm in three-dimensional one.

During the early stages of the loading, the maximum damage was detected near the outer edge of the central cross section. As the specimen is progressively stretched, the maximum damage area moves gradually towards the

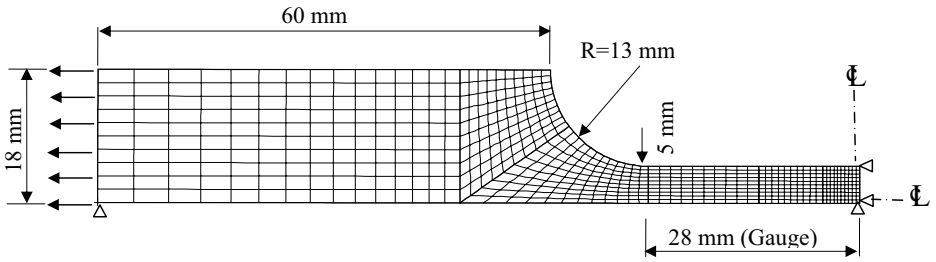

(a) Two-dimensional model

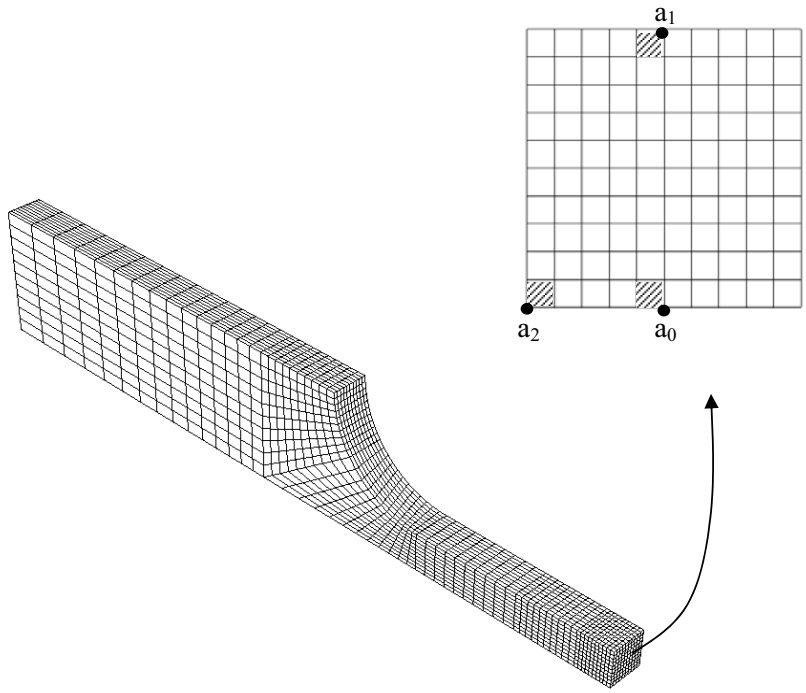

(b) Three-dimensional model

Figure 2 : A quarter of two- and three-dimensional tensile test models using symmetry condition.

Table 2 : Material data and Lemaitre damage model parameters for tensile test [Benallal, et al. (1987)]

E	210 GPa
ν	0.3
σ_Y^0	620
Hardening curve	$\sigma_Y(\varepsilon_{eq}^p) = 620 + 3300[1 - \exp(-0.4\varepsilon_{eq}^p)]$ MPa
r	3.5 MPa
s	1.0

core of the specimen (at a_0) and localises there. At the final stage with a displacement of 4.3 mm in two-dimensional model and 5.59 mm in three-dimensional model, damage was highly localised around the centre a_0. Therefore, it is expected that the fracture initiation should occur in this area. This prediction is in agreement with experimental observations by Hancock and Mackenzie (1976) which show that for certain tensile notched specimen configurations fracturing initiates at the centre of the specimen and propagates towards the outer edge.

The applied load versus load line displacement (LLD) for elastic-plastic (undamaged) and elastic-plastic-damage (damaged) models are shown in Figure 3. This shows the damage influence on the global behaviour of the structure because the softening caused by damage results on the decrease of the load carrying capacity of the structure. The progressive softening during the loading reflects the internal degradation on the material response. The Mises stress distribution for these two cases are compared in Figure 4. Both the undamaged and damaged three-dimensional models stretched to the same level of 5.59 mm. In the undamaged model, a uniform Mises stress distribution along the gauge length was observed without any necking. But in the damaged model the necking near the central part of the sample was formed and the Mises stresses were minimum at the core of the specimen (at a_0). Figure 5 shows the history of the evolution of Mises stress at three different location of a_0, a_1 and a_2 as marked on the sample cross section in Figure 2. Element a_0 at the core was at the highest strain and completely failed, i.e. $D > D_c$, while the edge elements at a_1 and a_2 still have load carrying capacity.

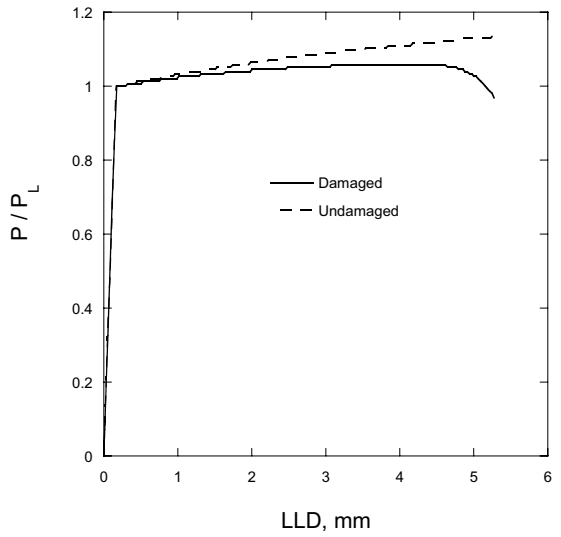

Figure 3 : Comparison of non-dimensional applied load vs. load line displacement in three-dimensional tensile test between damaged and undamaged models. ($P_L = 15500N$ is the limit load at first yield in tensile test).

The reason for faster damaging at the centre lies in the fact that damage growth in ductile metals is strongly dependent on the stress triaxiality ratio, p/σ_{eq}, which is highest at the centre of the specimen as shown in Figure 6. A marked decrease in ductility occurs as the triaxiality ratio increases. This phenomenon is captured by Lemaitre ductile damage model. Figure 7 shows the evolution of the triaxiality ratio during the loading history along $a_1 - a_0$ section. In the beginning of the process, the maximum damage is located on the outer surface. At later stage of loading, the triaxiality remains constant across the cross section at 1/3. However, as the load further increases, the triaxiality in 10% of the thickness close to the edge drops below 1/3, while in the remaining part of the section it increases above 1/3. Also the triaxiality growth rate is higher toward the centre. This causes the critical zone to move towards the centre of the specimen. This has a direct effect on damage parameter as illustrated in Figures 8 and 9.

The evolution of damage,D, and of effective plastic strain, $\dot{\varepsilon}^p_{eq}$, at the specimen centre, as the prescribed displacement increases with time is shown in Figure 8. It is interesting to note that, although initially the damage rate, $\dot{D}$, is slightly smaller than the rate of effective plastic strain, $\dot{\varepsilon}^p_{eq}$, as the displacement increases, the stress state at the centre of the specimen causes the damage to increase exponentially whereas the equivalent plastic strain rate remains approximately constant. This behaviour reflects the fact that $\dot{\varepsilon}^p_{eq} << \dot{D}$ near the failure site. For example by looking at Figure 9, the damage at the centre element a_0 is reached to 0.8 at stretching of 5.15 mm, while the damage at the outer element a_1 at the same stretching has only reached to 0.24.

6.2 Three Point Bending Test

In this example, three point bending test which have been extensively used in both experimental and numerical analysis were used to verify the damage model and its capability to predict the crack initiation site in the test.

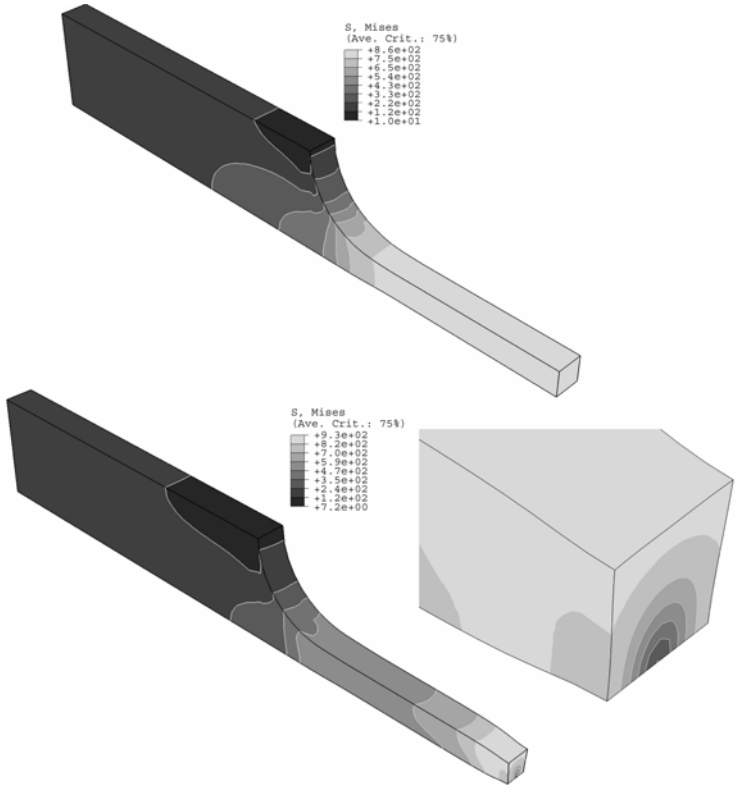

Figure 4 : Comparison of the Mises stress distribution from FEA (a) undamaged model, (b) damaged model.

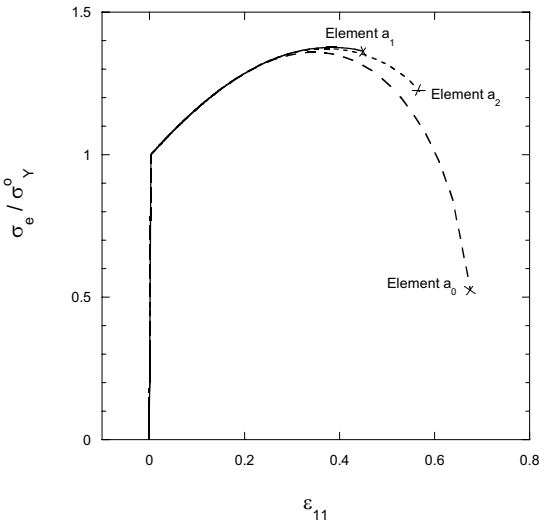

Figure 5 : Stress-strain in three-dimensional tensile test with damaged model at positions a_0, a_1 and a_2 shown in Figure 1 (the initial yield stress $\sigma_Y^0 = 620\,\text{MPa}$).

The specimen was made according to the ASTM Standard E399-90 (1994), except that it contained a straight-face notch terminated by a semicircular tip instead of a sharp crack. The geometry and FE mesh of the specimen are shown in Figure 10.

The dimensions and material properties for this example were chosen in accordance to tests carried out by Giovanola (1999). The material was high strength steel HY130 and the corresponding material properties were presented in Table 3. Since the experimental material coefficients s and r regarding to the damage evolution were not available for this material, $s = 1$ was chosen according to [Lemaitre (1996)] and values of $r = 1$, 5, 13 and 20 were tried for calibrating the FEA load-crack tip opening displacement (CTOD) with the experimental one. The final material properties which was obtained in this way and used in the damage evolution law were summarised in Table 3.

In developing the mesh using the plane of symmetry, only half of the specimen was discretised and the appropriate symmetric boundary conditions imposed to the relevant

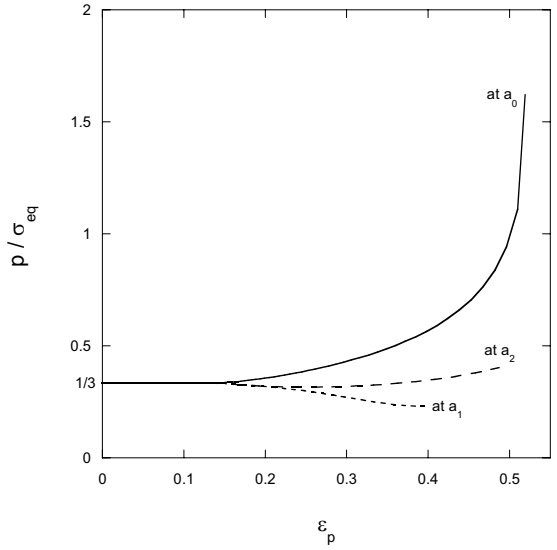

Figure 6 : Evolution of triaxiality, p/σ_{eq}, at a_0, a_1 and a_2 elements as shown in Figure 1 in three-dimensional tensile test model.

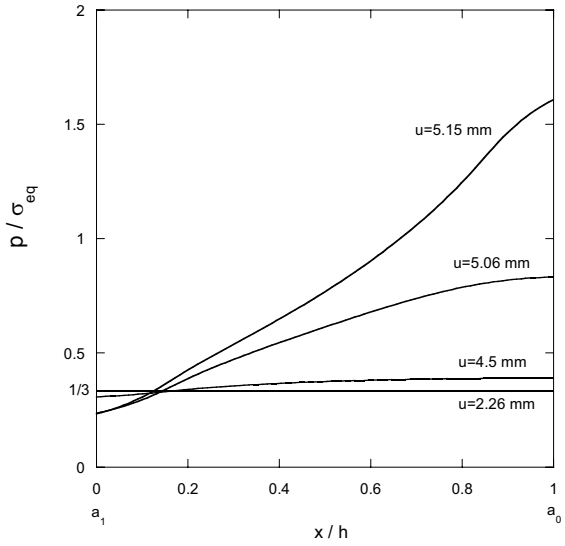

Figure 7 : Evolution of triaxiality, p/σ_{eq}, during the loading history along $a_1 - a_0$shown in Figure 1 in three-dimensional tensile test model.

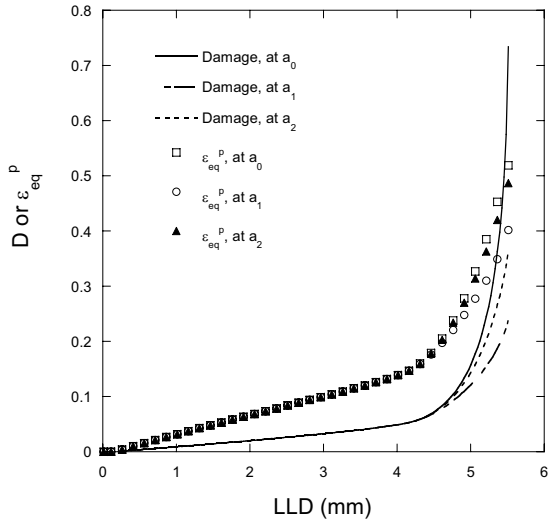

Figure 8 : Evolution of damage parameter, D, and equivalent plastic strain,ε^p_{eq}, at position a_0, a_1 and a_2 in three-dimensional tensile test model.

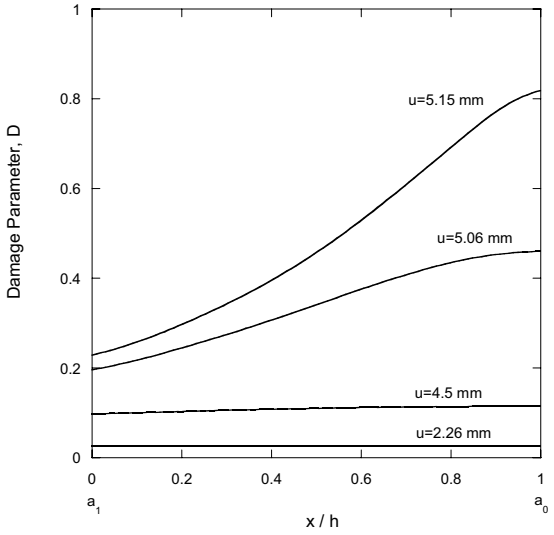

Figure 9 : Evolution of damage parameter, D, during the loading history along $a_1 - a_0$shown in Figure 1 in three-dimensional tensile test model.

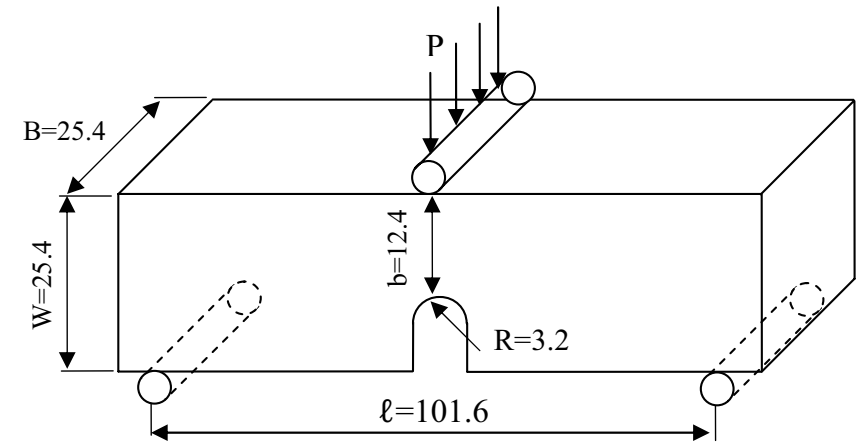

(a)

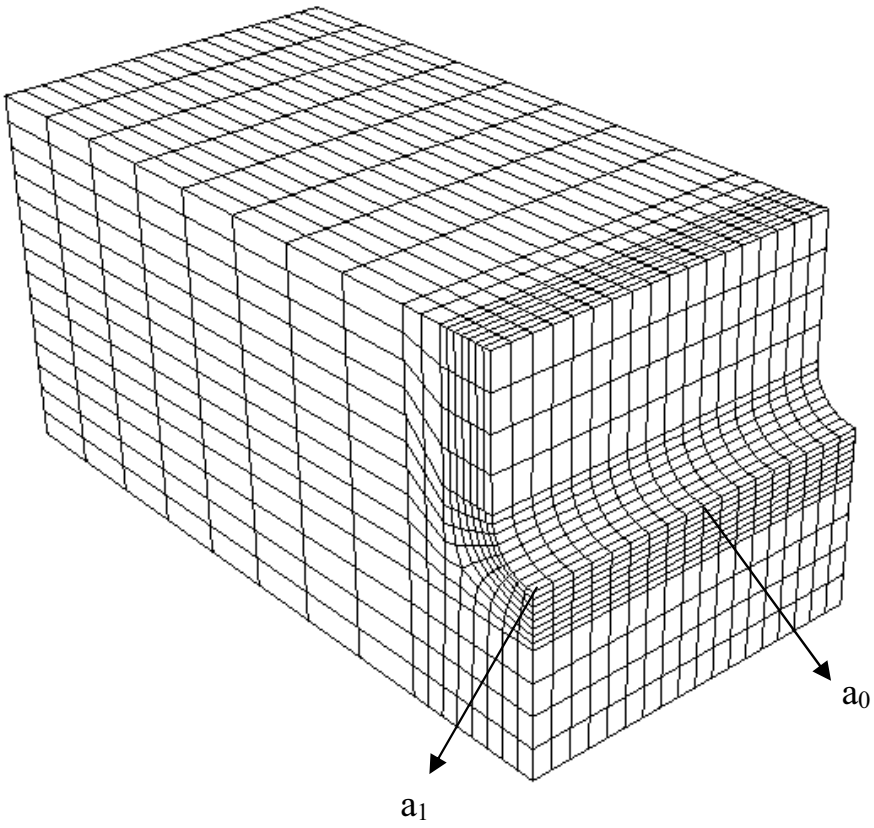

(b)

Figure 10 : Three point bending test. (a) Geometry and dimension (all in mm), (b) Finite element model of half of geometry using symmetry condition.

Table 3 : Material data and Lemaitre damage model parameters for high strength steel HY 130

E	176 GPa
ν	0.3
σ_Y^0	950
Hardening curve	$\sigma_Y(\varepsilon_{eq}^p) = 950 + 7600[1 - \exp(-0.55\varepsilon_{eq}^p)]$ MPa
r	13 MPa
s	1.0

edges. The FEA results will be compared with the experimental results presented previously [Giovanola, et al. (1999)].

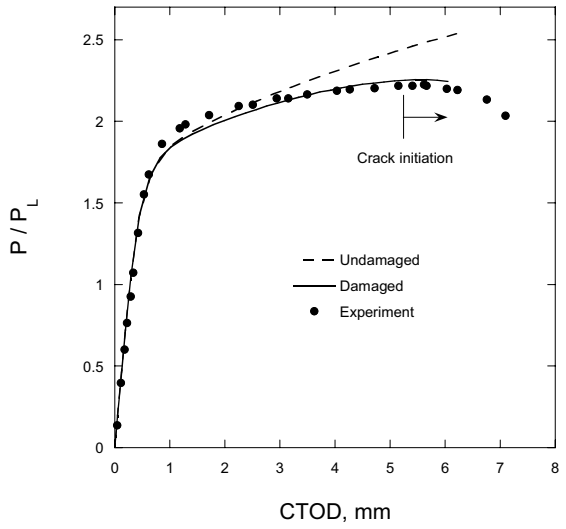

Figure 11 : Comparison of non-dimensional applied load vs. crack tip opening displacement in three-point bending test model between damaged and undamaged models and experiment from Giovanola et al. (1999) ($P_L = \frac{0.728Bb^2\sigma_Y}{\ell} = 27887.04N$ is the limit load at first yield in three-point bending test)

The applied load versus CTOD for undamaged and damaged models together with the experimental results from [Giovanola, et al. (1999)], are compared in Figure 11. It is possible to observe the damage influence on the global behaviour of the structure because the softening caused by damage decreases the load carrying capacity of the sample. The progressive softening during the loading reflects the internal degradation on the material response. The results of the damaged model agree quite well with the experiment. In fact, the position of experimentally detected crack initiation coincides with the damage growth of $D = 0.8$ at element a_0.

The damage contours plots at the Load-Line Displacement (LLD) of 0.43 mm and 8.8 mm are presented in Figure 12. During the early stages of the loading process, damage was grown uniformly across the notch. As the specimen is progressively deformed, the maximum damage area moves gradually toward the notch centre of the specimen. This is due to higher stress triaxiality ratio at the notch centre. As can be seen from Figure 13, the triaxiality initially grows both around the edge and at the centre of the notch. As the load on the specimen increases, the triaxiality remains nearly constant both at the centre and at the edge of the notch. At this stage, the magnitude of triaxiality at the centre element a_0 is more than 1.5 times its value at the edge element a_1. However, as shown in Figure 13, the damage parameter grows exponentially. At maximum applied load, the damage parameter at the centre element a_0 is about four times higher than the edge element a_1. The result is earlier damage localisation and deterioration of central region compared to the outer edges. This suggests that fracture initiation should be expected in this region. This result is in agreement with the experimental observations of Giovanola (1999), which reported fracture initiation at the centre of notch as shown in Figure 14a. The damage parameter at the load corresponding to experiment shown in Figure 14a is $D = 0.8$ at element a_0 and shown in Figure 14b.

7 Concluding remarks

Material degradation has been widely modelled by continuum damage mechanics and it is accepted as a reliable methodology. This paper dealt with the implementation of elastic-plastic-damage model in ductile fracture.

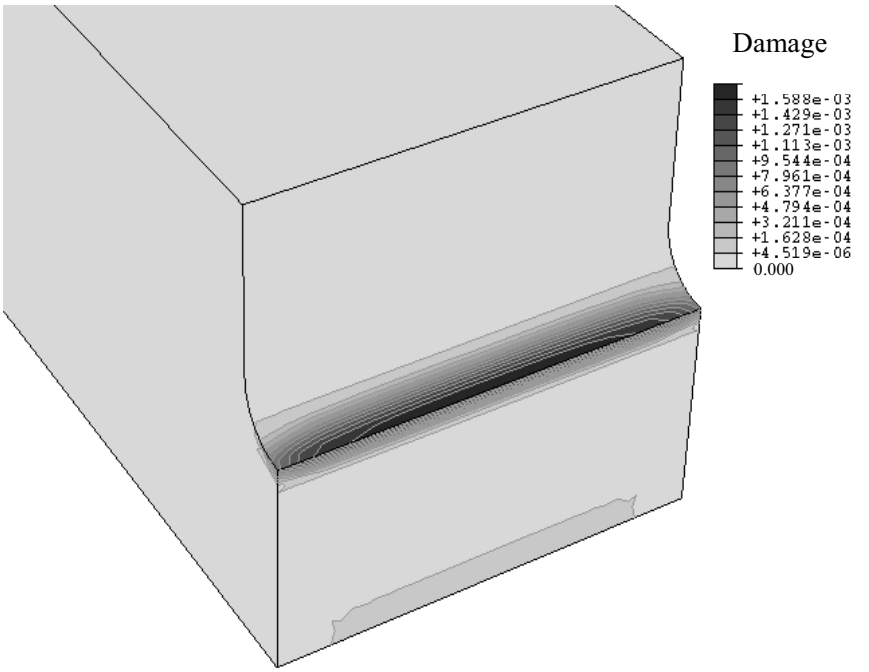

(a)

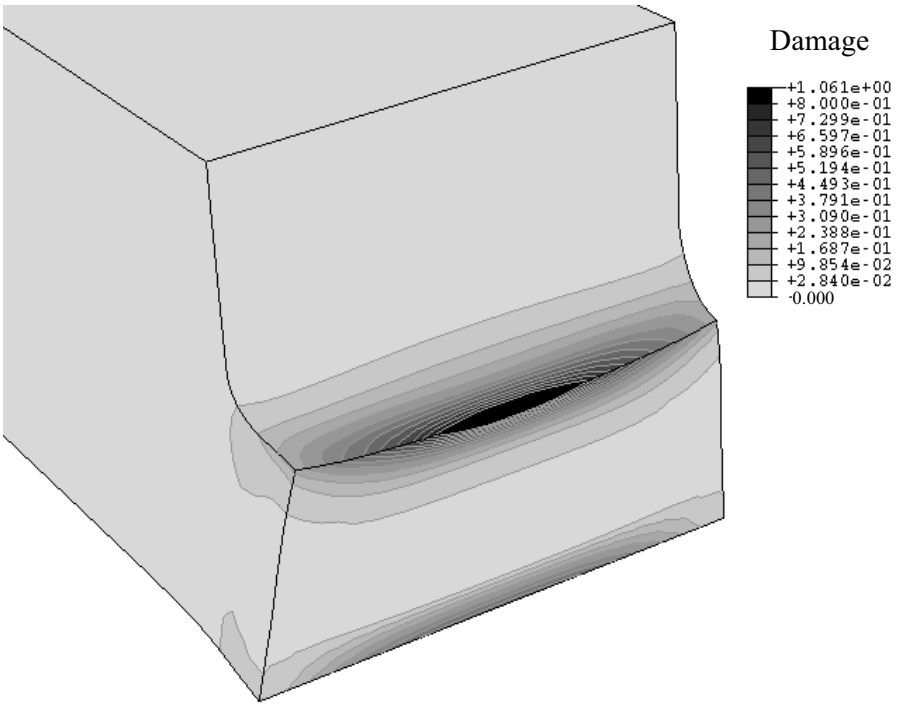

(b)

Figure 12 : Damage evolution in three-point bending test during the loading history, (a) At load line displacement of 0.43 mm, (b) At load line displacement of 8.8 mm.

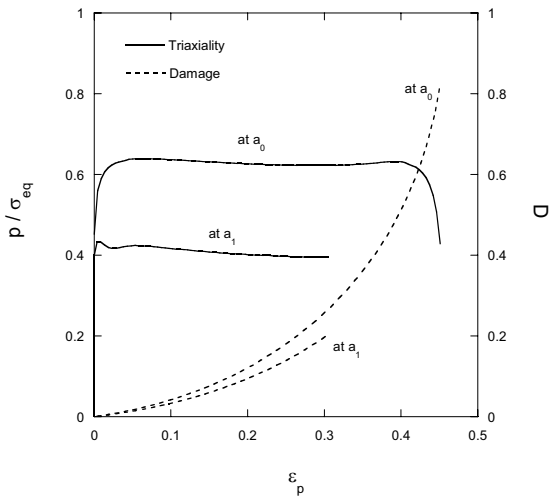

Figure 13 : Evolution of damage parameter, D, and triaxiality, at the centre element a_0 and edge element a_1 marked in Figure 9 in three-point bending test.

The coupled solution of evolution of plastic deformation and damage constitutive equation ensure a rigorous description of the interaction of the phenomena involved. In the numerical scheme the simple one-equation return mapping integration algorithm of de Souza Neto (2002) for the modified Lemaitre ductile damage model that ignores kinematic hardening effects has been used. Using the method, a computer code has been developed to solve damage growth in any two- and three-dimensional solids problem. In the present paper, two numerical examples were solved by this code. The results revealed different aspects of the model in regards to the rate of growth of equivalent plastic strain, triaxiality and damage parameter.

The model has been successfully used to predict the extent and the location of crack initiation sites. In the finite element analysis, it was assumed that cracks initiates at certain points in the geometry where the damage reaches the critical value, D_c. Good agreement for crack initiation site between numerical damage model and experiments on three point bending tests previously performed by Giovanola (1999) has been observed.

References

ABAQUS User's Manual Version 6.3. Habbitt Karlsson and Sorensen Inc., Providence, RI, USA, 2003.

ASTM Standard E 399-90. Standard test method for plane-strain fracture toughness of metallic materials. Annual Book of ASTM Standards, Section 3. vol. 03.01. Philadelphia, PA: American Society for Testing and Materials. 1994.

Andrade Pires, FM, Cesar de Sa, JMA, Costa Sousa, L, Natal Jorge, RM. (2003): Numerical modelling of ductile plastic damage in bulk metal forming, *Int J Mech Sci* **45**:273-294.

Benallal A, Billardon R, Dogheri I, Moret-Bailly L. (1987): Crack initiation and propagation analyses taking into account initial strain hardening and damage fields, Proceedings of the 4^{th} Int Conf of *Numerical Method in Fracture Mechanics,* Texas, USA, 337-351.

Chaboche JL. (1988a): Continuum damage mechanics: Part I-General concepts. *Journal of Applied Mechanics* **55**:59–64.

Chaboche JL. (1988b): Continuum damage mechanics: Part II-Damage growth, crack initiation, and crack growth. *Journal of Applied Mechanics* **55**:65–72.

de Souza Neto EA, Peric D, Owen DRJ. (1994): A model for elastoplastic damage at finite strains: algorithmic issues and applications. *Engineering Computations*, **11**(3):257–81

de Souza Neto, EA. (2002) A fast one-equation integration algorithm for the Lemaitre ductile damage model, *Commun. Numer. Meth. Engrg.* **18**:541–554.

Giovanola JH, Kirkpatrick SW, Crocker JE. (1999): Fracture of Geometrically Scaled Notched Three-Point-Bend Bars of High Strength Steel, *Journal of Engineering Fracture Mechanics*, **62**(2-3):291-310.

Hancock JW, Mackenzie AC. (1976): On the mechanisms of ductile fracture in high-strength steels subjected to multi-axial stress-states. *Journal of the Mechanics and Physics of Solids* **24**:147–69.

Kachanov, LM. (1958): On the time to failure under creep conditions. *Izv. AN SSSR, Otd. Tekhn. Nauk* **8**:26-31.

Krajcinovic D, Fonseka GU. (1981): The continuous damage theory of brittle materials, part I: general theory. *Journal of Applied Mechanics, Transactions of American Society of Mechanical Engineers*, **48**:809–15.

Krajcinovic D. (1983): Constitutive equations for damaging materials. *Journal of Applied Mechanics, Transactions of American Society of Mechanical Engineers*,

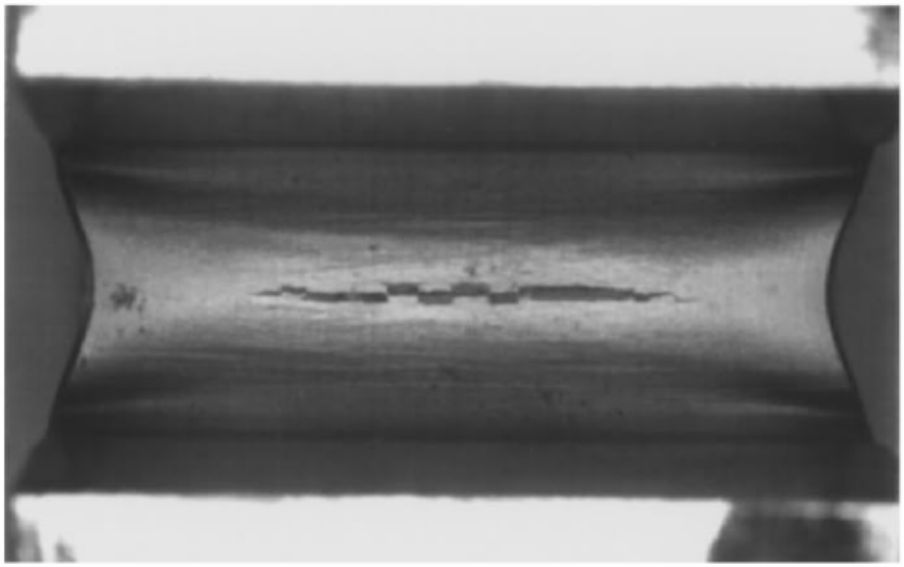

(a)

(b)

Figure 14 : Comparison of experimental Giovanola et al. (1999) crack initiation site in three-point bending test with damaged finite element solution. $D = 0.8$ at the notch centre.

50:355–60.

Krajcinovic D, Selvaraj S. (1984): Creep rupture of metals—an analytical model. *Journal of Engineering Materials and Technology, Transactions of American Society of Mechanical Engineers* **160**:809–15.

Lemaitre, J. (2001): *Handbook of Materials Behavior Models*, Academic Press.

Lemaitre J. (1984): How to use damage mechanics. *Nuclear Engineering and Design* **80**:233–45.

Lemaitre J. (1985a): A continuous damage mechanics model for ductile fracture. *Journal of Engineering Materials and Technology, Trans ASME,* **107**:83–89.

Lemaitre J. (1985b): Coupled elasto-plasticity and damage constitutive equations. *Computer Methods in Applied Mechanics and Engineering* **51**:31–49.

Lemaitre J. (1996): A course on damage mechanics. Berlin, Heidelberg, New York: Springer.

Murakami S. (1988): Mechanical modeling of material damage. *Journal of Applied Mechanics* **55**:280–6.

Murakami S, Kamiya K. (1997) Constitutive and damage evolution equations of elastic-brittle materials on irreversible thermodynamics. *International Journal of Mechanical Sciences* **39**:473–86.

Murakami S. (1990): Role of continuum damage me-

chanics in fracture analysis. In: Kleiber M, Konig JA, editors. *Inelastic solids and structures*. Swansea: Pineridge Press, 67–80.

Saanouni K, Chaboche JL, Bathias C. (1986): On the creep crack growth prediction by local approach. *Engineering Fracture Mechanics* **25**:677–91.

Simo JC, Ju JW. (1987a): Strain and stress based continuum damage models-I. Formulation. *International Journal of Solids and Structures* **23**(7):821–40.

Simo JC, Ju JW. (1987b): Strain and stress based continuum damage models-II. Computational aspects. *International Journal of Solids and Structures* **23**(7):841–69.

Simo JC and Hughes TJR. (1998): Computational Inelasticity, Springer-Verlag, New York.

Vaz Jr. M. and Owen DRJ. (2001): Aspects of ductile fracture and adaptive mesh refinement in damaged elasto-plastic materials, *Int. J. Numer. Meth. Engrg.* **50**:29–54.